Robust Controller Design for a Parallel Resonant Converter Using μ-Synthesis

Juanyu Bu, *Student Member, IEEE,* Mario Sznaier, *Member, IEEE,* Zi-Qin Wang, and Issa Batarseh, *Senior Member, IEEE*

***Abstract*—DC-to-dc resonant converters have been the object of much attention lately. These converters have the potential to provide high-performance conversion without some of the problems associated with classical pulse-width modulation (PWM)-based converters, thus allowing for smaller, lighter power supplies. However, in order to achieve this, a suitable control circuit, capable of maintaining the desired output voltage under different operating conditions, is required. In the past, small signal models obtained around the nominal operating points were used to design controllers that attempted to keep the output voltage constant in the presence of input perturbations. However, these controllers did not take into account either load or components variations, and thus could lead to instability in the face of component or load changes. Moreover, the prediction of the frequency range for stability was done *a posteriori*, either experimentally or by a trial-and-error approach. In this paper we use μ-synthesis to design a robust controller for a conventional parallel resonant converter. In addition to guaranteeing stability for a wide range of load conditions, the proposed controller rejects disturbances at the converter input while keeping the control input and the settling time within values compatible with a practical implementation. These results are validated by means of detailed nonlinear circuit simulations obtained using P-spice.**

***Index Terms*—Resonant converters, robust control, μ-synthesis.**

I. Introduction

TRADITIONALLY, dc-to-dc power conversion has been based upon the use of switching-mode circuits, controlled using pulse-width modulation (PWM) techniques [1]. In PWM converters, the switching of the power semiconductor devices is done under high current levels. Hence, in order to reduce switching losses, the operating frequencies of these converters are limited. Furthermore, the high-frequency harmonic components due to the quasi-square switching current and/or voltage waveforms produce high levels of electromagnetic interference (EMI) [2], [3].

In contrast, in resonant converters the capacitor voltage and inductor current waveforms exhibit sinusoidal behaviors, allowing for higher operating frequencies. These high operating frequencies result in smaller, lighter magnetic components and faster transient responses. As a matter of fact, today's dc-to-dc resonant converters have their operating frequencies well in the megahertz range [4], with power density up to 50 W/in^3. Another advantage of resonant converters over PWM converters is the substantially lower harmonic content.

These features, combined with a steadily increasing demand for smaller size and lighter weight high-performance dc-to-dc converters in industrial, residential, and aerospace applications, have resulted in widespread interests in high-frequency resonant converters.

Depending on how energy is transformed from the resonant tank (LC) to the output circuit, these resonant converters are classified as *series* [5]–[12] and *parallel* [5], [7], [10]–[17] resonant converters. In the series type the energy is coupled from the inductor current to the output circuit, whereas in the parallel type the energy is transferred from the capacitor voltage or inductor voltage. In both types, the resonant tank (LC) plays the role of buffering the energy from the source to the output circuit.

The steady-state and dynamic behaviors of both the conventional series and parallel resonant converters have been thoroughly analyzed [2], [7], [8], [13], [14], [16], [18]. This analysis shows that series resonant converters require a wide range of switching frequencies in order to compensate for small load variations. Hence, they are preferred in applications with tight load regulations [6], [9], [16]. Unlike the series type ones, parallel resonant converters are more attractive to applications that need to accommodate a wide range of load variations [14], [15], [17].

It is well known that parallel resonant converters can operate in two modes: continuous conduction mode (CCM) [7], [13], [14] and discontinuous mode (DM) [19], [20]. Compared to CM converters, discontinuous mode operating converters have lower losses, due to zero-current and zero-voltage commutations occurring at internally controlled switching instants. However, this is achieved at the price of high current and voltage peaks that can cause intensive device stress. From a controller design standpoint, the presence of internally controlled switching instants renders the analysis of the operation of DM converters far more involved than in the CM case [19]. Additionally, since the voltage input–output transfer ratio is highly dependent on the load resistance, it is difficult to accommodate a wide range of loads.

Finally, quantum parallel resonant converters (QPRC's) [21] have been recently proposed as alternatives to conventional PRC's. QPR converters can be controlled to have nearly zero device voltage switching stresses and switching losses. However, modeling and controlling of these converters is difficult, due to their discontinuous switching modes and

Manuscript received May 20, 1996; revised December 12, 1996. Recommended by Associate Editor, K. D. T. Ngo. An abridged version of this paper was presented at the 1994 PESC. This work was supported in part by NSF under Grant ECS-9211169.

J. Bu, M. Sznaier, and Z.-Q. Wang are with the Electrical Engineering Department, Pennsylvania State University, University Park, PA 16802 USA.

I. Batarseh is with the Electrical Engineering Department, University of Central Florida, Orlando, FL 32816-2450 USA.

Publisher Item Identifier S 0885-8993(97)06399-0.

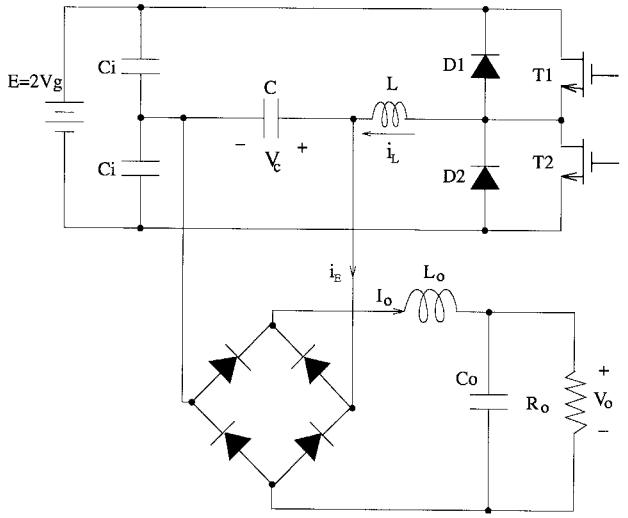

Fig. 1. The conventional second-order PRC circuit diagram.

quantized characteristics resulting in highly nonlinear output voltage versus load and switching conditions characteristics.

For the reasons mentioned above, in this paper we will concentrate only on parallel resonant converters operating at continuous conduction mode. Several techniques commonly used to control CCM PRC's were compared in [22]. As shown there, most of these techniques have a relatively poor performance. A proposed alternative control law is the optimal trajectory control method, which achieves good nominal performance, but entails using a complex, nonlinear controller.

Recently, small signal models obtained using perturbation methods have been used to design controllers that attempt to keep the output voltage constant in the presence of input perturbations [23]. However, these controllers did not take into account either load or component variations. Moreover, prediction of the admissible load range for stability was done *a posteriori*, either experimentally or by a trial-and-error approach.

In this paper, we use μ-synthesis (see [24] and [25] and references therein) to design a robust controller for a conventional CCM PRC. The design objective is to robustly reject input variations in the presence of load and component uncertainties, while keeping both control actions and settling time small. This is accomplished by selecting appropriate weight functions reflecting these requirements.

This paper is organized as follows. In Section II, we briefly describe the conventional PRC and we provide a small signal model around the nominal operating point. In Section III, we analyze the characteristics of the plant. This analysis provides some insights into the nature of the control problem, in particular displaying the relatively poor control characteristics of the plant. In Section IV, we indicate how to characterize plant uncertainty and we design a robust controller to achieve robust performance (i.e., guaranteed performance for all possible plants) using μ-synthesis. In Section V, we provide linear and nonlinear simulation results showing the performance of the closed-loop system under different conditions. Finally, in Section VI, we summarize our results.

II. Problem Description

A. The Conventional Parallel Resonant Converter

Fig. 1 shows a diagram of a conventional second-order PRC [23]. The combinations of the diodes and transistors form bidirectional switches operating at 50% duty ratio. Thus, in each switching period the resonant circuit L-C is alternatively excited by $+V_g$ and $-V_g$. The large output inductor L_o and capacitor C_o are used to minimize the load effect on the resonant capacitor voltage and to ensure the constant output voltage through the output circuit [13]. As for notation, the resistor R_o and the voltages V_g and V_o represent the load, the line (input) and the output, respectively.

Throughout this paper we will use as nominal parameters the following values, taken from the design example in [13, ch. 2]:

$$\begin{aligned} L &= 41.18\ \mu\text{H} \\ C &= 11.30\ \text{nF} \\ R_o &= 208.33\ \Omega \\ L_o &= 10\ \text{mH} \\ C_o &= 47\ \mu\text{F} \\ V_g &= 100\ \text{V} \\ V_o &= 250\ \text{V} \\ f_s &= 200\ \text{kHz} \\ Z_o &= \sqrt{L/C} = 60.39\ \Omega. \end{aligned}$$

For convenience, we introduce the following normalized variables:

$$\begin{aligned} V_{ng} &= \frac{V_g}{V_g} = 1 \\ Q_p &= \frac{R_o}{Z_o} = 3.45 \\ V_{no} &= \frac{V_o}{V_g} = 2.5 \\ F_{ns} &= \frac{f_s}{f_o} = 0.86 \end{aligned}$$

where the resonant frequency $f_o = 1/2\pi\sqrt{LC}$.

B. Small Signal Model

Under steady-state conditions it can be shown that, for a PRC operating in the continuous conduction mode [23], there are four circuit modes in each switching period. Thus the converter is a nonlinear variable structure system, with its steady-state trajectory uniquely determined by the normalized switching frequency F_{ns} and the load condition Q_p [11]. For a given operating point, a discrete-time small signal model of the converter can be obtained by using a perturbation method [23]. The sampling time for this discrete-time model is equal to $T_s/2$, where $T_s = 1/f_s$ is the switching period. Therefore, it follows that this model is correct under small signal perturbations with frequencies up to the operating switching frequency $\omega_s = 2\pi f_s = 1.26 \cdot 10^6$ rad/s.

The discrete-time model from the normalized switching frequency F_{ns} and the normalized line V_{ng} to the normalized output V_{no} (to simplify the notation, we use the same variables for both the steady state and its perturbation) at the nominal operating point is given by the following state-space realization [23]:

$$X(k+1) = AX(k) + BU(k)$$
$$V_{no}(k) = CX(k)$$

where

$$A = \begin{pmatrix} 0.8219 & 0.5504 & -2.1402 \\ -0.2767 & 0.6108 & -0.6644 \\ 0.0053 & 0.0075 & 0.9387 \end{pmatrix}$$
$$B = \begin{pmatrix} -6.4684 & 0.4834 \\ 10.6774 & 1.9499 \\ -0.0002 & 0.0162 \end{pmatrix}$$
$$C = 0 \quad 0 \quad 3.45.$$

The state variables and inputs are defined as

$$X(k) = [i_{nl}(k) \quad v_{nc}(k) \quad I_{no}(k)]^T$$
$$U(k) = [F_{ns}(k) \quad V_{ng}(k)]^T$$

where i_{nl}, v_{nc}, and I_{no} are the normalized resonant inductor current, capacitor voltage and output current, respectively.

C. Control Objectives

Fig. 2 illustrates the diagram used for control design. In the small signal model of the converter there are two inputs: line voltage V_{ng} and switching frequency F_{ns}. The switching frequency F_{ns} will be used as the control input to the plant. The objective is to synthesize a controller having as input the error signal (obtained by comparing the output voltage versus the reference input r) and as output the switching frequency, such that the output voltage is kept at a prescribed level (in our case, $V_o = 250$ V, i.e., $V_{no} = 2.5$) at all operating points. This problem can further be divided into four parts.

1) Line regulation (nominal performance). The line voltage is often unregulated and could have a substantial range of variation, typically around $\pm 20\%$. This variation will be modeled as an external disturbance, thus leading to a disturbance rejection problem. Performance specifications for this type of problems are usually given in terms of time-domain quantities, such as:
   a) zero steady-state error;
   b) small overshoot at output (usually less than 10% for reference input step response);
   c) appropriate settling times for both line and reference inputs step responses (5 ms at most in our case);
   d) a closed-loop bandwidth of at least 360 Hz in order to successfully suppress line ripple.
2) Load regulation (robust stability). On the other hand, the load condition could also vary over a wide range. Since the load R_o enters the dynamics of the model, load variations will appear as model uncertainty and could possibly lead to stability problems. Normally the load changes from 10% at low load to 90% at full load condition. Other model uncertainties, such as unmodeled high-frequency dynamics and uncertainties in the resonant inductor L and capacitor C, will also be considered.
3) Robust performance. Since the converter operates at a wide range of load conditions, the performance requirements must be satisfied at all operating points. This is equivalent to requiring satisfactory response under both line and load variations.
4) Finally, in order to guarantee implementability of the resulting controller, all physical variables must be limited to practical values. Due to the high sampling rate (roughly 200 kHz) of the plant, a digital implementation of the controller would require a specialized digital signal processor (DSP), with enough processing power to carry out the required operations in a very short period of time. As an alternative to the sampling and hold (S/H) circuitry, the controller will be implemented with an analog circuit consisting of a VCO and other analog devices.

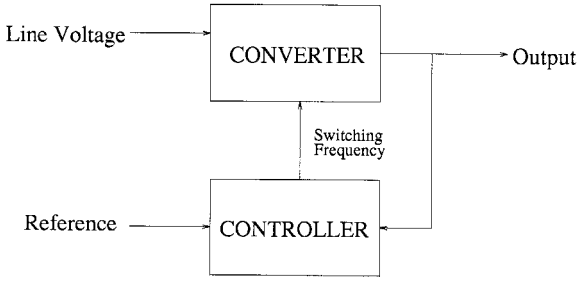

Fig. 2. The diagram for control design.

III. Analysis of the Plant

A. Control Characteristics

For a PRC converter operating in steady-state conditions, the input–output relationships can be represented by the control characteristics curves, relating the output voltage to the load and switching frequency. Given any two variables among the normalized output V_{no}, switching frequency ratio F_{ns} and

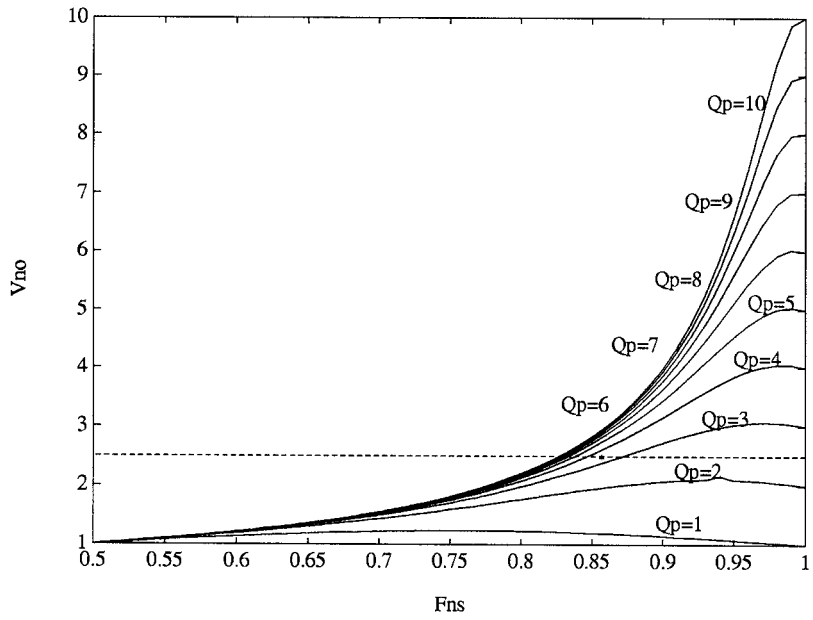

Fig. 3. The conventional PRC control characteristics curves.

output load Q_p, the third variable can be determined from the curves. Thus, these curves allow for easily visualizing the effects of the switching frequency and the load upon the converter output. From a control point of view, the control characteristics curves allow us to make an initial estimate of the load change that can be tolerated and to see some of the difficulties inherent to the load regulation problem.

Fig. 3 shows the control characteristics curves for various output loads Q_p, obtained analytically from the steady-state analysis. To maintain the output voltage constant in the presence of perturbations, the controller should adjust the switching frequency to keep the converter operating along the dashed line indicated in Fig. 3. As the converter is perturbed away from the nominal operating point (marked with a * in the figure) the plant dynamics may vary significantly. As pointed out in [23], this relatively poor control characteristics result in a difficult control problem.

Remark 1: Note that from Fig. 3 it follows that at lighter loads (higher R_o, larger Q_p and lower I_o), a small frequency change will result in larger output changes. Thus, we should expect that the control problem will become more difficult at larger Q_p values. In the next section we will show, through a frequency domain analysis, that this is exactly the case.

B. Frequency Responses

From the discrete-time state-space model, we can easily get the z-transfer functions from the normalized switching frequency F_{ns} and the normalized line input V_{ng} to the normalized output V_{no}

$$[G(z)G_g(z)] = \begin{bmatrix} \dfrac{V_{no}(z)}{F_{ns}(z)} & \dfrac{V_{no}(z)}{V_{ng}(z)} \end{bmatrix} = C[zI - A]^{-1}B. \quad (1)$$

Following a common approach, we will carry out the analysis of the plant and the synthesis of a digital controller using a w-plane approach [26]. To this effect, the bilinear transformation

$$z = \frac{1 + sT_s/4}{1 - sT_s/4} \quad (2)$$

is used to get the transfer functions in the frequency domain s. These transfer functions, still denoted as $G(s)$ and $G_g(s)$, are given by

$$G(s) = 2.652 * 10^{-2} \cdot \frac{(s + 795\,041)(s - 792\,431)(s - 800\,003)}{(s + 29\,167)(s + 83\,363 \pm 202\,487i)} \quad (3)$$

$$G_g(s) = -1.367 * 10^{-2} \cdot \frac{(s - 800\,003)(s + 484\,930 \pm 290\,253i)}{(s + 29\,167)(s + 83\,363 \pm 202\,487i)}. \quad (4)$$

The above transfer functions correspond to the nominal load $R_o = 208.33\ \Omega$. As stated before, since the load enter the dynamics of the converter, load variations result in different transfer functions. Figs. 4 and 5 show the frequency responses of $G(s)$ and $G_g(s)$ corresponding to several different load conditions, respectively.

These figures show that as the load becomes lighter (larger R_o), the overshoot increases, leading to a more difficult control problem. This conclusion is consistent with the conclusion drawn in the last section from the study of the control characteristics. On the other hand, the control characteristics require that Q_p be greater than V_{no} in order to get the prescribed output voltage. Since in our design example the value of V_{no} is chosen to be 2.5, it follows that R_o should be greater than 151 Ω. Therefore, in the sequel we will assume that R_o varies within the range 151–1200 Ω.

IV. Control Design

As mentioned in Section II, our goal is to design a controller that satisfies the performance specifications listed there for all load conditions in the range 151 $\Omega \leq R_o \leq$ 1200 Ω,

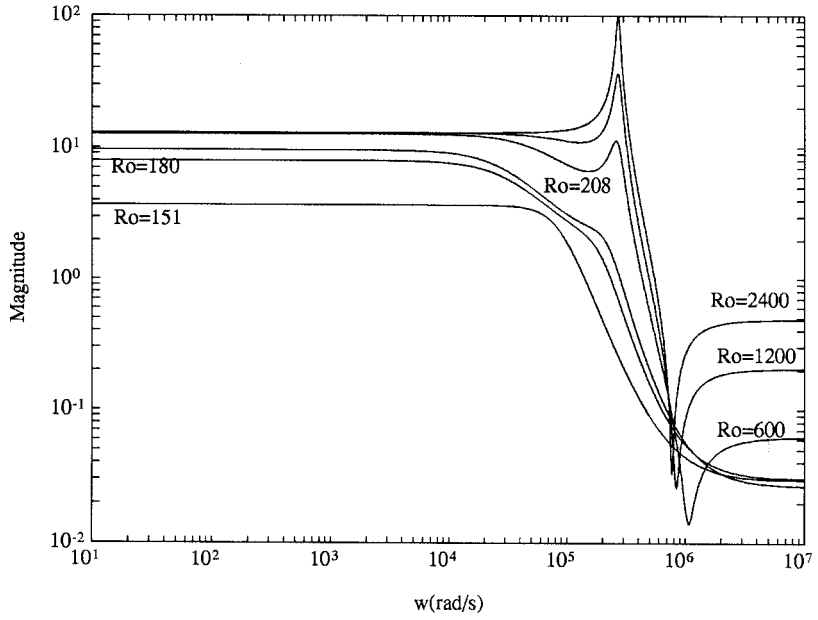

Fig. 4. Frequency responses $G(s)$ at different load conditions.

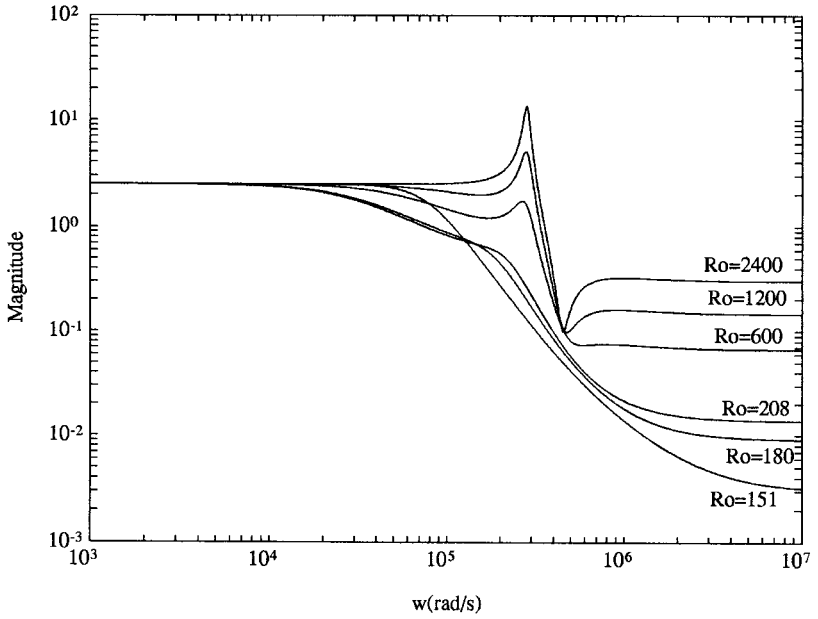

Fig. 5. Frequency responses $G_g(s)$ at different load conditions.

assuming that the values of the components of the resonant tank are known within a 10% tolerance. In the sequel we will solve this problem by recasting it into a robust performance synthesis form and using μ-synthesis [27]. To this effect we need first to describe the family of plants corresponding to different values of the load as a nominal plant subject to uncertainty, as described in the next section.

A. Plant Description and Uncertainty Weight Selection

In this paper we will address the model uncertainty caused by load variations by using a single, norm bounded, multiplicative uncertainty to cover all possible plants as follows: Let $G^{R_o}(s)$ and $G_g^{R_o}(s)$ denote the transfer functions from the control input and line input to the output at operating points other than the nominal point ($R_o \neq 208.33\ \Omega$), respectively. Following a practice common in robust control, we will represent these transfer functions as

$$G^{R_o}(s) = G(s)(1 + \Delta_I(s)W_I(s)) \tag{5}$$

$$G_g^{R_o}(s) = G_g(s)(1 + \Delta_g(s)W_g(s)) \tag{6}$$

where $G(s)$ and $G_g(s)$ are the nominal transfer functions given in (3) and (4), respectively, $W_I(s)$ and $W_g(s)$ are fixed weighting functions containing all the information available about the frequency distribution of the uncertainty, and where $\Delta_I(s)$ and $\Delta_g(s)$ are stable transfer functions representing

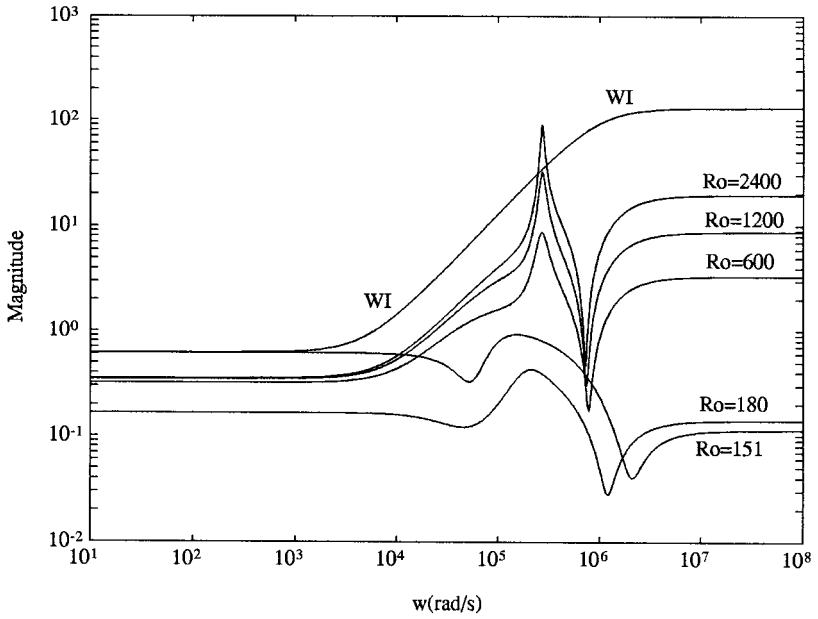

Fig. 6. Multiplicative uncertainties (control to output) and weight.

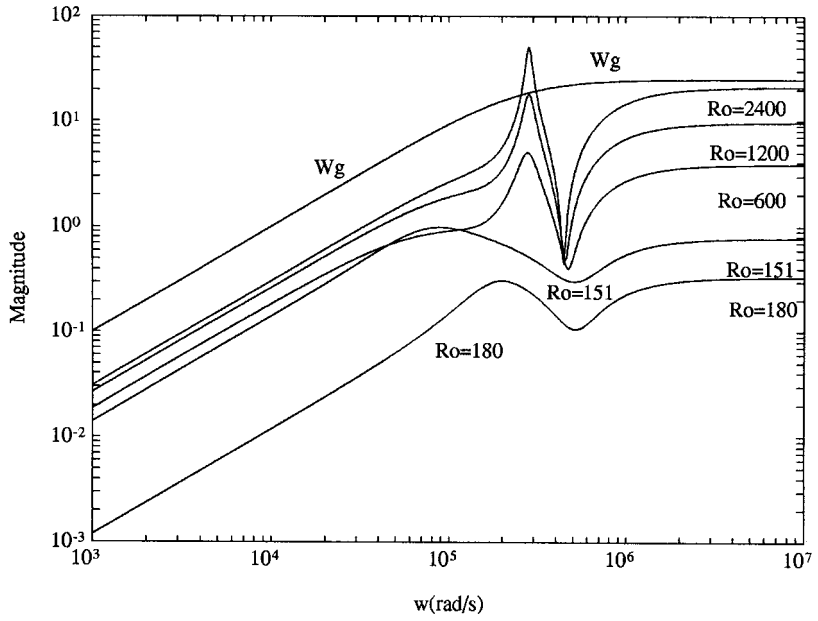

Fig. 7. Multiplicative uncertainties (line to output) and weight.

model uncertainty. Furthermore, without loss of generality (by absorbing any scaling factor into $W_I(s)$ and $W_g(s)$ if necessary), it can be assumed that $||\Delta_I(s)||_\infty \leq 1$ and $||\Delta_g(s)||_\infty \leq 1$, where $||\Delta(s)||_\infty \doteq \sup_\omega |\Delta(j\omega)|$. Thus, $W_I(s)$ and $W_g(s)$ are such that their respective magnitude Bode plots cover the Bode plots of all possible plants. Some sample uncertainties corresponding to different values of the load R_o are shown in Figs. 6 and 7. We can see that in both figures the multiplicative uncertainties have a peak around the resonant frequency. This peak becomes larger and steeper as the load resistance R_o increases.

Based on these plots, the following multiplicative uncertainty weights were chosen for control design (see [28] for more details on uncertainty weight selection):

$$W_I(s) = \frac{1.4 * 10^{-4}s + 0.65}{10^{-6}s + 1} \tag{7}$$

$$W_g(s) = \frac{10^{-4}s}{4 * 10^{-6}s + 1}. \tag{8}$$

The magnitude frequency responses of $W_I(s)$ and $W_g(s)$ are also shown in Figs. 6 and 7, respectively. These figures clearly show that attempting to cover the sharp peak around the resonant frequency will result in large gaps between the weight and the uncertainty at high frequencies, introducing conservatism at that frequency range. On the other hand, a tighter fit at high frequencies using higher order functions will

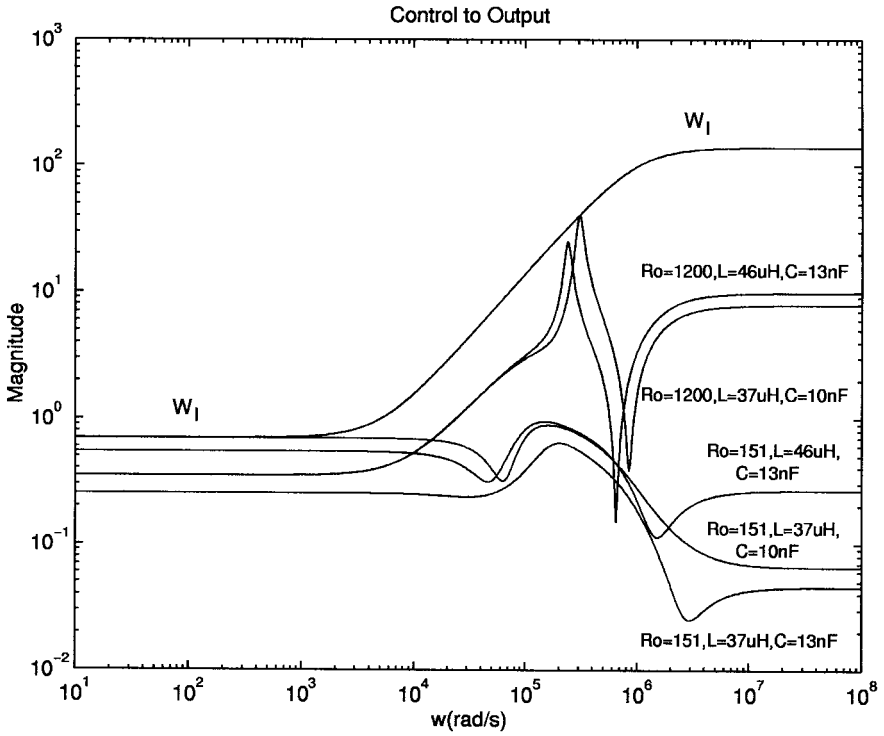

(a)

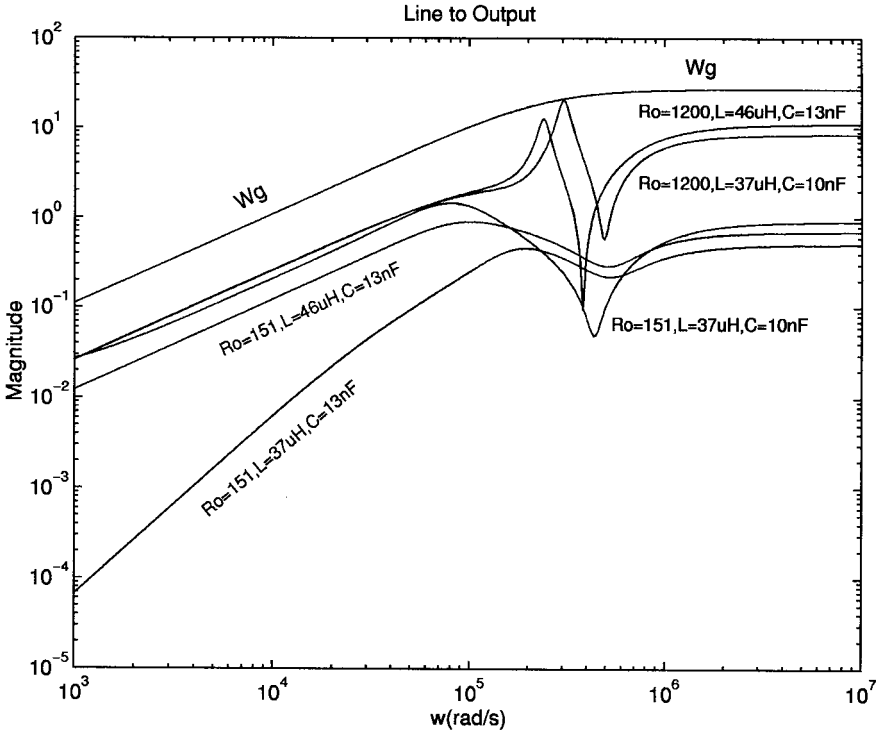

(b)

Fig. 8. Uncertainties due to $\pm 10\%$ changes of L and/or C at extreme load conditions $R_o = 1200$ and $151\ \Omega$.

result in high-order controllers. The weights (7) and (8) used in our design provide a good tradeoff between robustness and controller complexity.

We turn our attention now to the effects of changes in the values of L and C, the resonant tank components. Since these changes affect the location of the resonant peak, they could conceivably destabilize any controller designed based upon its nominal location. Fig. 8 shows the changes in the transfer functions due to $\pm 10\%$ changes in the values of L and/or C. It is worth noticing that our choice of weighting functions W_I and W_g will also cover this family of plants, even at the extreme load conditions $R_o = 1200$ and $151\ \Omega$. Thus, a robust

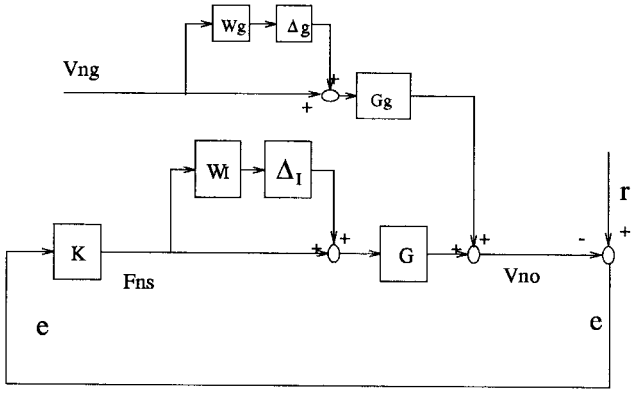

Fig. 9. The block diagram of the converter including the uncertainty due to load and component variations.

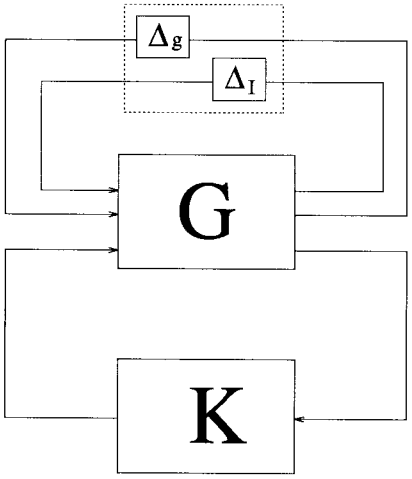

Fig. 10. Block diagram with the uncertainty "pulled" out of the loop.

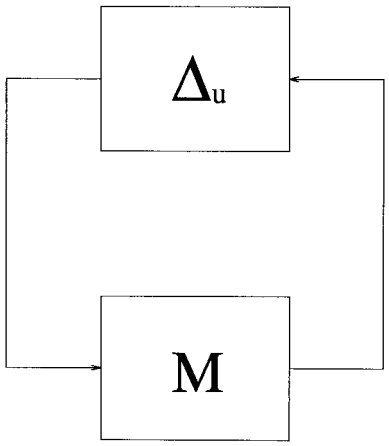

(a)

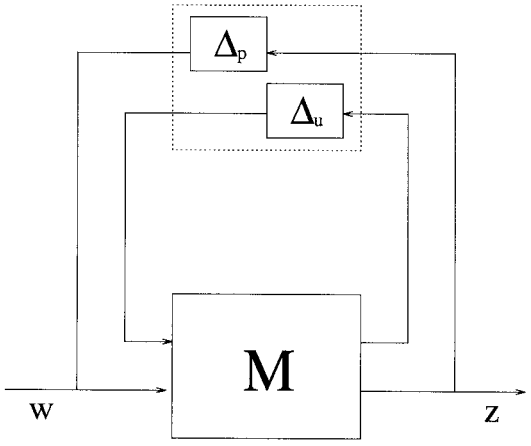

(b)

Fig. 11. (a) Robust stability problem. (b) Robust performance as a robust stability problem.

controller designed using these weighting functions will be able to accommodate both changes in the load condition and uncertainty in L and C.

Fig. 9 shows a block diagram of the converter, taking into account the uncertainty. By "pulling" the uncertainty out of the loop, this diagram can be recast in the form shown in Fig. 10, where G represents the nominal converter (including the weights W_I and W_g), K is the controller to be designed, and where the combined uncertainty $\Delta(s) = \text{block} - \text{diag}\{\Delta_I(s), \Delta_g(s)\}$ has a block diagonal structure. Designing a controller K to stabilize a system of this form is a standard robust control problem that can be solved using μ-synthesis. In the next section, for the sake of completeness, we briefly cover the fundamentals of this method. Interested readers are referred to [24] and [25] for a more detailed discussion of the history and theory of both μ and μ-synthesis.

B. Structured Singular Value and μ-Synthesis

Consider the generalized system interconnection shown in Fig. 11, consisting of a stable transfer function matrix M (in our case the combination of the nominal converter G and the controller K) and a "feedback" term Δ_u, representing model uncertainty with a block diagonal structure of the form

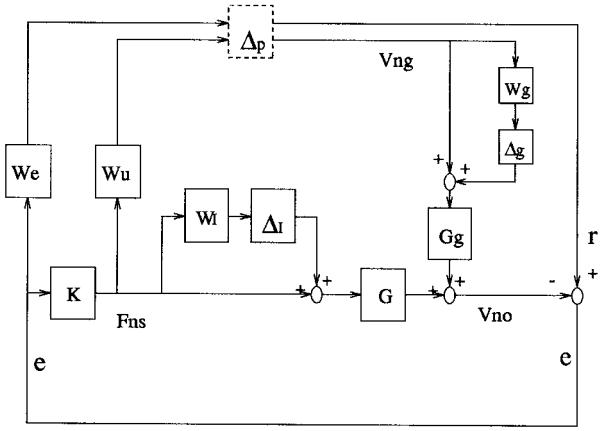

Fig. 12. The block diagram for μ-synthesis.

(see [29])

$$\Delta_u(s) \in \boldsymbol{\Delta} \equiv \{\Delta(s) = \text{block} - \text{diag}\{\Delta_1(s), \Delta_2(s) \cdots, \Delta_n(s)\}, \Delta_i(s) \text{ stable}\}. \quad (9)$$

The stability of this interconnection has been analyzed in [29]–[31]. In [20] and [31], Safonov and Athans defined the

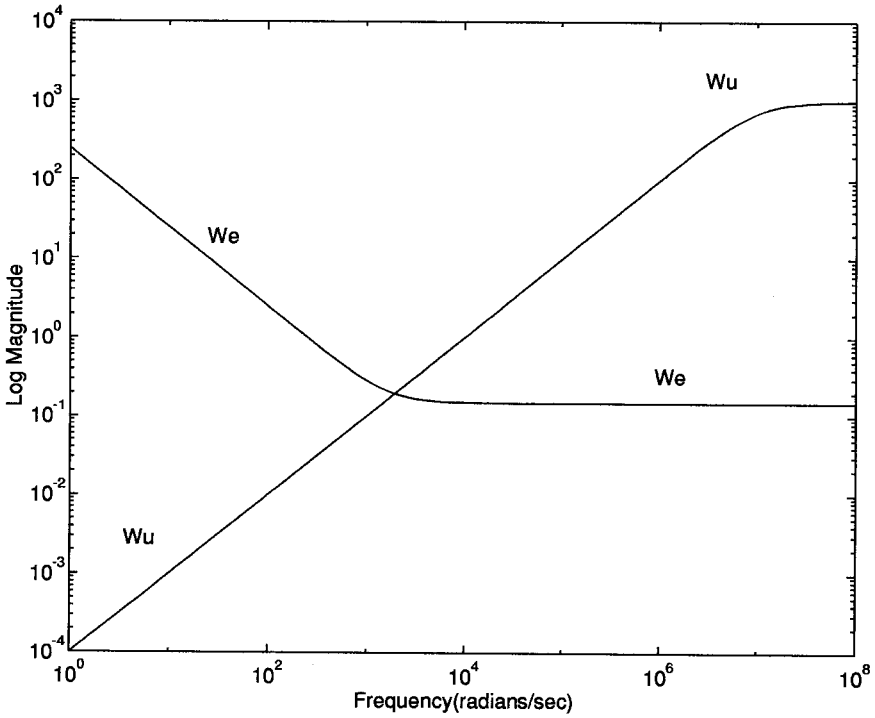

Fig. 13. Performance weights $W_e(s)$ and $W_u(s)$.

multivariable stability margin k_m as the largest positive k_m such that the interconnection is stable for all $\Delta, \|\Delta\|_\infty \leq k_m$, i.e.,

$$k_{m_{\Delta_u}}(M) = \min_{\Delta_u \in \boldsymbol{\Delta}} \{\|\Delta_u\|_\infty : \det(I + M(j\omega)\Delta_u(j\omega)) = 0 \text{ for some } \omega\} \tag{10}$$

where $\|\Delta_u\|_\infty \equiv \sup_w \overline{\sigma}(\Delta_u)$ and where $\overline{\sigma}(\cdot)$ denotes the maximum singular value. Thus, k_m is an indicator of the largest uncertainty permissible before instability occurs. In [29], Doyle introduced the concept of structured singular value (SSV or μ), defined as shown in (11) at the bottom of the page. Hence, μ is simply equal to the reciprocal of k_m.

As shown in [29], if M is a stable transfer matrix, the necessary and sufficient condition for robust stability of the interconnected system for all perturbations $\|\Delta_u\|_\infty \leq 1$ is that

$$\mu_{\Delta_u}(M) < 1.$$

Robust performance (i.e., guaranteed performance for all possible plants in the set) can be addressed by recasting the problem into an augmented robust stability problem by introducing an additional fictitious perturbation block Δ_p, as shown in Fig. 11(b), where w and z represent exogenous inputs and outputs subject to performance specifications, respectively. It can be shown (see the main loop theorem in [25]) that *robust performance* is achieved if and only if

$$\mu_{RP} = \sup_\omega \mu_\Delta(M) < 1$$

where $\Delta = \text{diag}\{\Delta_p, \Delta_u\}$ contains now both the uncertainty and the performance blocks.

μ provides a useful tool for robustness analysis that combines unstructured and structured uncertainty, robust stability, and robust performance in a unified, nonconservative, framework. It can even be extended to cover parametric uncertainty (real μ). Unfortunately, at the present time there are no efficient algorithms for computing the exact value of μ for general perturbation structures. Instead, the following upper bound is used [29], [31]:

$$\mu_\Delta(M) \leq \inf_{D \in \mathcal{D}} \|DMD^{-1}\|_\infty \tag{12}$$

where $\mathcal{D}$ represents a set of positive definite hermitian matrices with a diagonal block structure that commutes with that of Δ. It can be shown that problem (12) can be recast as a convex optimization problem, leading to efficient computational algorithms. Moreover, this upper bound coincides with the exact value of μ for perturbation structures having up to three blocks. For more than three blocks, the bound is no longer tight. However, the largest gap ever observed is less than 15% (corresponding to an example built analytically), and is substantially lower in most cases arising in practice [25].

$$\mu_{\Delta_u}(M) = \begin{cases} \dfrac{1}{\min_{\Delta_u \in \boldsymbol{\Delta}} \{\|\Delta_u\|_\infty : \det(I + M(j\omega)\Delta_u(j\omega)) = 0 \text{ for some } \omega\}} \\ 0 \text{ if no } \Delta_u \in \boldsymbol{\Delta} \text{ destabilizes } M \end{cases} \tag{11}$$

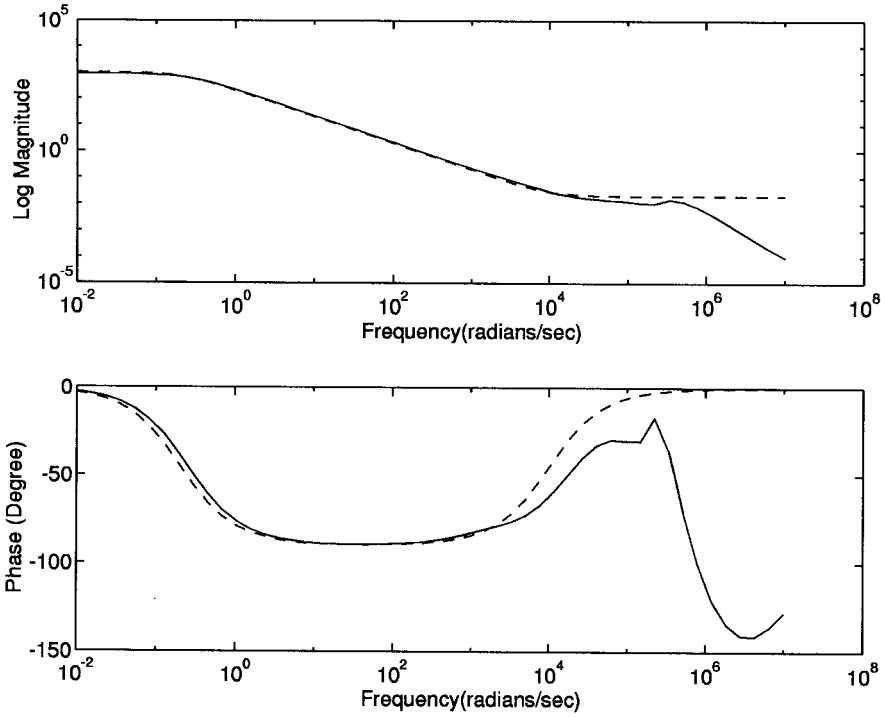

Fig. 14. Frequency responses of μ (solid) and phase-lag (dash) controllers.

From the discussion above it follows that controllers guaranteeing robust stability or robust performance can be synthesized by solving the following optimization problem:

$$\min_{\text{K stabilizing}} \mu_{\Delta}\{M(K)\}$$

where the notation $M(K)$ is used to indicate explicitly that the closed-loop transfer matrix M is a function of the controller K. Due to the difficulties in computing the exact value of μ, the upper bound (12) is used instead, yielding the following optimization problem (in K and D)

$$J = \min_{\text{K stabilizing}} \{\inf_{D\in\mathcal{D}} \|DM(K)D^{-1}\|_{\infty}\}. \qquad (13)$$

Robust stability or robust performance is achieved if $J<1$.

While the optimization problem (13) is convex either in the scales D or in the controller K, *it is not jointly* convex in D and K. Thus, there potentially exist local minima where an optimization algorithm may get trapped. The solution method currently used alternates between finding the tightest possible upper bound by optimizing the scales D while holding the controller constant (an infinite dimensional convex optimization problem); and finding an internally stabilizing controller that minimizes this upper bound (a standard $\mathcal{H}_{\infty}$ control problem). This algorithm, known as the "$D-K$" iteration, is implemented both in the Robust Control Toolbox [32] and μ Analysis and Synthesis Toolbox [32], and can be summarized as follows.

1) $\mathcal{H}_{\infty}$ synthesis. Holding D fixed, use $\mathcal{H}_{\infty}$ synthesis to solve

$$\min_{\text{K stabilizing}} \|DM(K)D^{-1}\|_{\infty}. \qquad (14)$$

In the first iteration D is often set to I(identity matrix). After the first iteration the D scale obtained in Step 3) is used.

2) μ analysis. Calculate the upper bound of μ for the closed-loop system obtained using the controller K from Step 1). This entails solving the following infinite dimensional optimization problem:

$$\inf_{D\in\mathcal{D}} \|DM(K)D^{-1}\|_{\infty}. \qquad (15)$$

This problem is approximately solved by finding the value of D over a finite grid of frequency points ω_i.

3) D fitting. The approximate solution to the optimal scaling problem of Step 2) is found by fitting the values $D(j\omega_i)$ with a real-rational, proper, stable, minimum-phase transfer matrix $D(s)$. Note that the order of the controller is that of the augmented plant (plant + weights) $+2\times$ order of D. Thus, in order to obtain controllers with reasonable complexity, the order of D should be kept low (usually first or second order).

4) Go to Step 1) until the stop criterion is met, which means that the condition $J<1$ is satisfied.

As mentioned before, while due to the lack of joint convexity in K and D, this algorithm is not theoretically guaranteed to converge to the global minimum, it works well in practice, and has allowed for solving many difficult engineering problems (see, for instance, [33]).

C. Performance Weight Selection

Fig. 12 shows the block diagram used for μ-synthesis in our case. As discussed in Section IV-A, here Δ_I and Δ_g are scalar blocks, representing the model uncertainty perturbations from the control and line inputs respectively, and W_I and W_g are

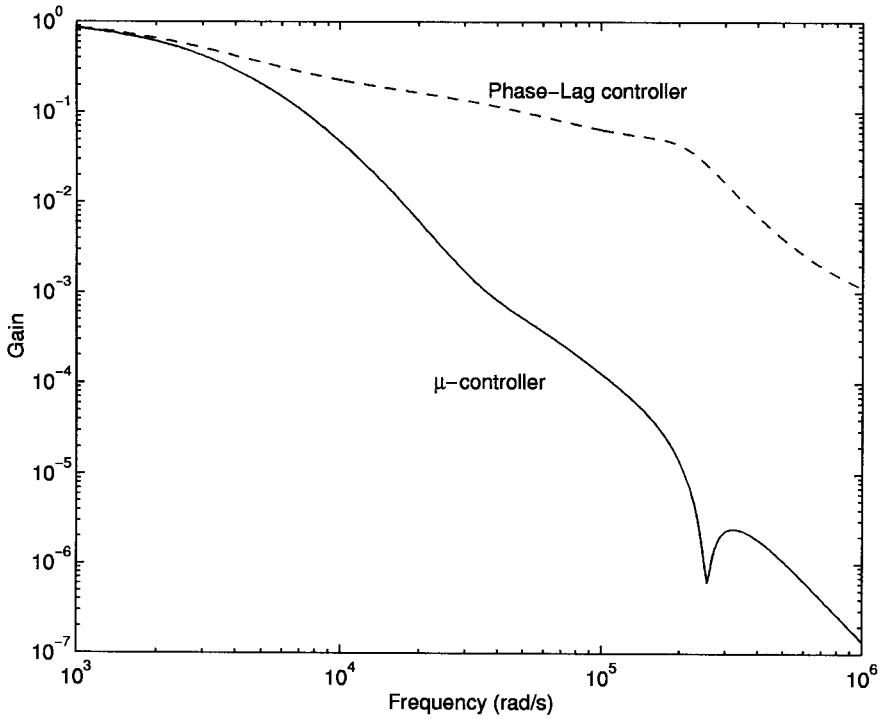

(a)

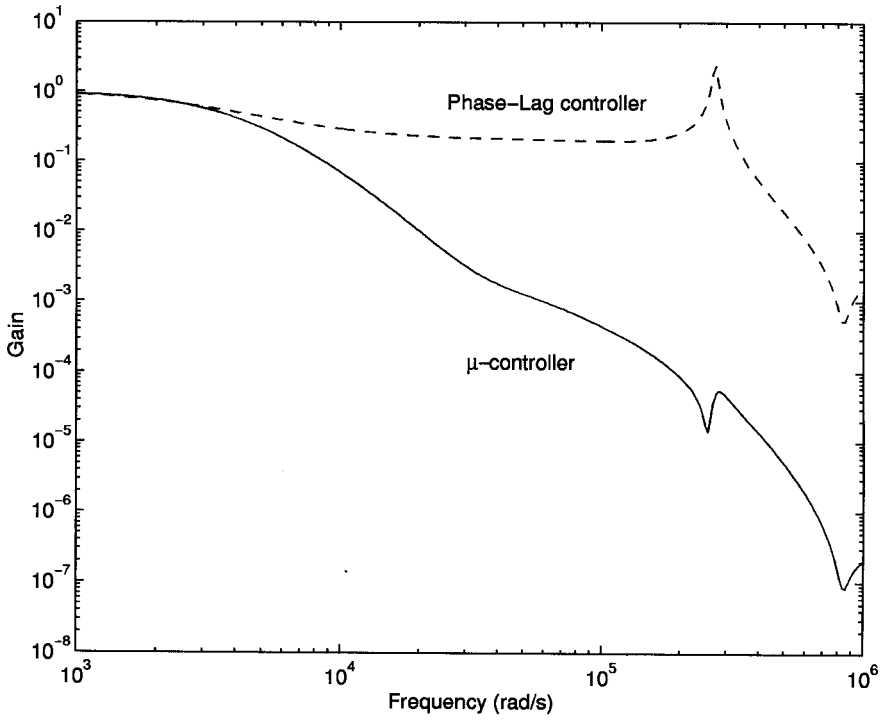

(b)

Fig. 15. Closed-loop frequency responses for μ (solid) and phase-lag (dash) controllers: (a) $R_o = 208\ \Omega$ and (b) $R_o = 1200\ \Omega$.

the corresponding uncertainty weights. As we discussed in the last section, in order to guarantee robust performance we need to add to this structure an additional (fictitious) uncertainty block Δ_p, along with the corresponding performance weights W_e and W_u, associated with the tracking/regulation error and the control effort, respectively. In this Section, we briefly describe the method used to select these weights. Note in passing that since the line input is modeled as a disturbance input, the associated uncertainty block Δ_g can be absorbed into the performance block Δ_p to further simplify the problem. However, this will introduce unnecessary conservatism in the design.

The selection of $W_e(s)$ and $W_u(s)$ entails a tradeoff among different performance requirements, specifically good regula-

tion versus peak control action. The weight on the control error $W_e(s)$ is usually selected to be very large at low frequencies in order to get good tracking and regulation. Additionally, as pointed out in Section IV-B, the order of the weights should be kept low in order to keep the controller complexity low. A good compromise between performance and complexity is given by weighting functions of the form

$$W_e(s) = \frac{T_1 s + 1}{T_2 s + A} \tag{16}$$

where A is the desired steady-state error (A will be zero if zero steady-state is required); T_1 approximately determines the bandwidth ($\omega_b \approx 1/T$) and hence the rising time and settling time; where the ratio T_2/T_1 is associated with performance requirements against high-frequency noise (see [34] and references therein for more details). Note that there is no exact relationship between the parameters T_1 and T_2 and time domain performance specifications given in terms of rise-time, settling-time, and overshoot. The design of multiobjective robust controllers subject to both time and frequency domain specifications is, to a large extent, an open problem, although some progress has been made recently (see [35] and references therein).

When using frequency domain weights to enforce time-domain specifications, an initial guess could be made based on classic control methods. Usually, an iterative procedure alternating between weight selection, controller synthesis, and performance evaluation is then conducted in order to obtain a satisfactory design. When all the performance specifications are met but there is still room left for improvement, usually we only improve T, in order to get a response as fast as possible, while still satisfying other specifications.

Based on this discussion, the following weights, offering a good compromise among all the conflicting time–domain specifications, were selected:

$$W_e(s) = \frac{0.0006s + 1}{0.004s} \tag{17}$$

$$W_u(s) = \frac{10^{-4}s}{10^{-7}s + 1} * = . \tag{18}$$

Here the weight on the control input $W_u(s)$ was chosen close to a differentiator to penalize fast changes and large overshoot in control input. These weights give a closed-loop bandwidth of approximately $1/0.0006 \approx 1700$ rad/s. Note that with this $W_e(s)$ zero steady-state error will be achieved. We may relax this performance requirement if we allow for a small, nonzero, steady-state error. The frequency responses of $W_e(s)$ and $W_u(s)$ are shown in Fig. 13.

D. Controller Synthesis

By using the uncertainty description developed in SectionIV-A and the performance weights of Section IV-C, we get an uncertainty structure Δ consisting of two scalar blocks (corresponding to the robust stability requirements) and a 2×2 block (corresponding to the robust performance requirements). Note that in this case, since the Δ structure has only three blocks, the upper bound of $\mu, \inf_{D \in \mathcal{D}} \|DMD^{-1}\|_\infty$, coincides with its exact value. The robust controller was synthesized using the μ Analysis and Synthesis Toolbox [27], applied to the block diagram shown in Fig. 2. After four $D-K$ iterations with third-order D-scalings, we obtained a 18th-order controller yielding $\mu_{RP} = 0.9721$. Finally, Hankel norm model reduction yielded a sixth-order controller with virtually no performance degradation ($\mu_{RP} = 0.9753 < 1$). The state-space description of this reduced order controller is given by

$$K = C_k(sI - A_k)^{-1}B_k + D_k \tag{19}$$

where we have the equations shown at the bottom of the page.

In order to benchmark the performance of the robust controller, we also designed a phase-lag controller using classical design tools, based on the plant frequency responses at the various operating points shown in Fig. 4. To improve performance, this controller was further tuned by trial and error. The transfer function of the final controller is given by

$$K_{pl} = \frac{0.02s + 200}{s + 0.2}. \tag{20}$$

The frequency responses of both the μ and the phase-lag controllers are shown in Fig. 14. Both controllers have similar responses at low frequencies, while at high frequencies the gain of the μ controller decays faster in order to accommodate the model uncertainties at high frequencies.

Fig. 15 shows the closed-loop frequency responses for the nominal plant and for the lightest load considered in the design. Note that in both cases the μ controller provides lower gain and better rolloff at high frequencies. Moreover, while the response corresponding to the phase-lag controller is acceptable for the nominal plant, it exhibits a large peak at the resonant frequency

$$A_k = \begin{pmatrix} -0.25 & 1.708 & -1.144 & 1.414 & -0.1161 & 1.296 \\ 1.708 & -1.320e+5 & 9.980e+4 & -3.190e+5 & 1.460e+4 & -2.213e+5 \\ -1.144 & 9.980e+4 & -7.670e+4 & 3.208e+5 & -1.200e+4 & 1.983e+5 \\ -1.414 & 3.190e+5 & -3.208e+5 & -2.874e+5 & 1.729e+5 & -4.053e+5 \\ -1.161 & 1.460e+4 & -1.200e+4 & -1.729e+5 & -2.664e+3 & 1.013e+5 \\ -1.296 & 2.213e+5 & -1.983e+5 & -4.053e+5 & -1.013e+5 & -8.045e+5 \end{pmatrix}$$

$$B_k^T = (-2.338 \quad 7.983 \quad -5.345 \quad -6.610 \quad -0.543 \quad -6.060) \times 10^{-2}$$

$$C_k = (-0.935 \quad 3.193 \quad -2.138 \quad 2.644 \quad 0.217 \quad 2.424) \times 10^{4}$$

$$D_k = 0.$$

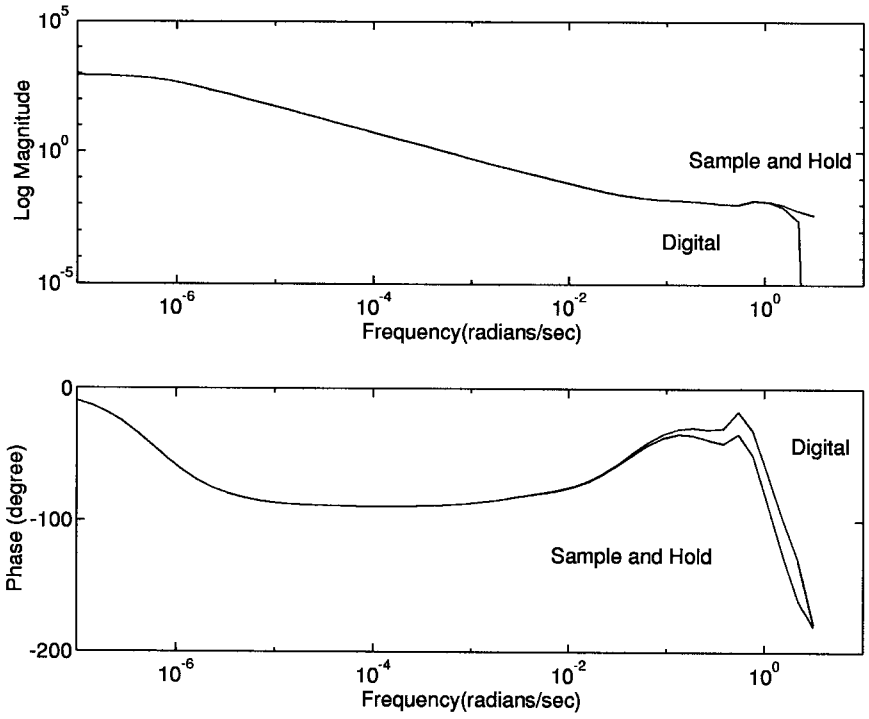

Fig. 16. Frequency responses of the digital and sampled controllers.

at light loads. As we will show in Section V, this peak results in significant performance deterioration at these loads.

E. Controller Implementation

Given the relatively high sampling rate (roughly 200 kHz), of the plant, a digital implementation of the sixth-order z-domain controller may require a specialized DSP processor, with enough processing power to carry out the required operations in a very short period of time. As an alternative, we propose to implement this controller using an analog, continuous-time controller, connected to the plant through sample and hold devices. Fig. 16 shows the frequency response of the μ-controller obtained by using the bilinear transform to convert the s-domain controller to the z-domain, versus the frequency response of the z-domain controller obtained by simply sampling the inputs and outputs of (19). From the figure it follows that both responses are quite close, due to the fact that the sampling frequency is much higher than the bandwidth of the controller. Moreover, notice that the converter itself provides a sample and hold action. Thus, connecting the s-domain controller directly to the plant should provide a response closely resembling that of the true z-domain μ-controller. This is the case as we will show in Section V-B through the use of a nonlinear simulation of the closed-loop system.

V. Simulation Results

A. Linear Simulation

The closed-loop system corresponding to the μ controller was simulated at the nominal operating point $R_o = 208\ \Omega$ and at two extreme cases $R_o = 151$ and $1200\ \Omega$, using the corresponding linear model of the plant. The time responses to 20% step change in line voltage V_{ng} and reference input r are shown in Fig. 17.

For the nominal case $R_o = 208\ \Omega$, the settling time is about 2.5 ms for both line voltage change and reference input change. The output responses are satisfactory since the settling time is smaller than the required 5 ms, with no overshoot. The control action in these responses is also adequate, without overshoot or abrupt change. This is due to the choice of the weight W_u, penalizing fast changes and overshoots in the control action.

When the operating point moves to $R_o = 151\ \Omega$, the settling times for both step changes are about 4 ms. This increase is mainly due to the significant decrease in plant static gain (see Fig. 4). The μ controller is undertuned at this operating point in order to achieve robust performance. When the operating point moves toward lighter loads, the responses are almost the same as the nominal, except that for the case $R_o = 1200\ \Omega$ (note that this load is the lightest load considered in our design), some chattering in both the output and control input starts to show off at the beginning of the responses. The occurrence of the chattering is linked to the large peak in the plant frequency response at lighter loads, barely covered by the uncertainty weights W_I and W_g.

From the simulation results it follows that the controller achieves robust performance, since all performance specifications are satisfied at all operating points of interest. However significant variation of performance is also observed. This is a direct result of the large variation in the plant dynamics, and any fixed linear controller can do very little in this respect. To reduce this variation will require using a nonlinear, gain scheduling controller.

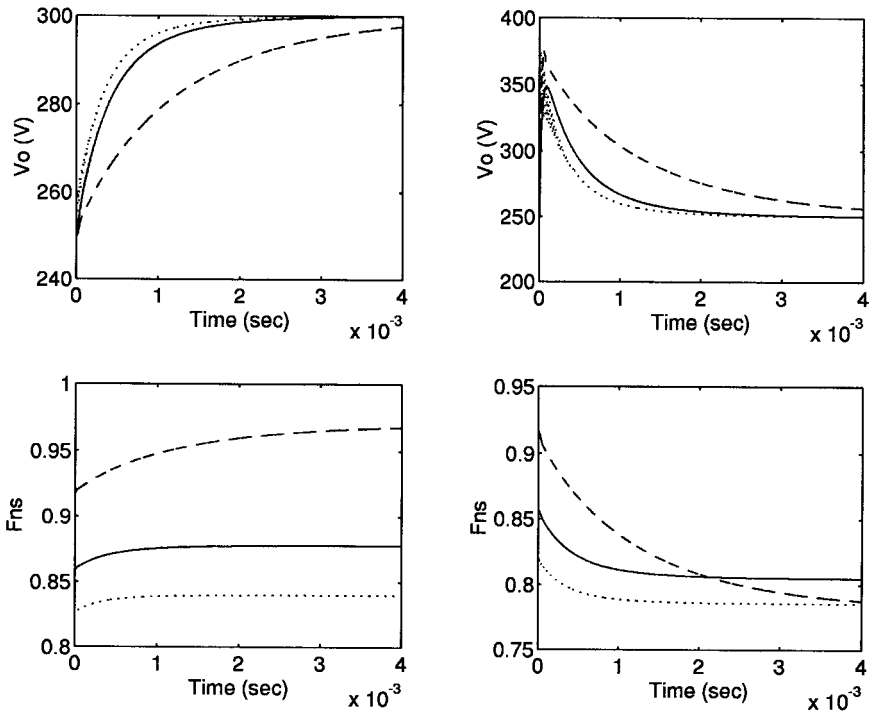

Fig. 17. Linear simulation results with μ controller at different operating points $R_o = 208$ (solid), 151 (dash), and 1200 (dot) Ω. (a) Reference input step change (20%). (b) Line voltage step change (20%).

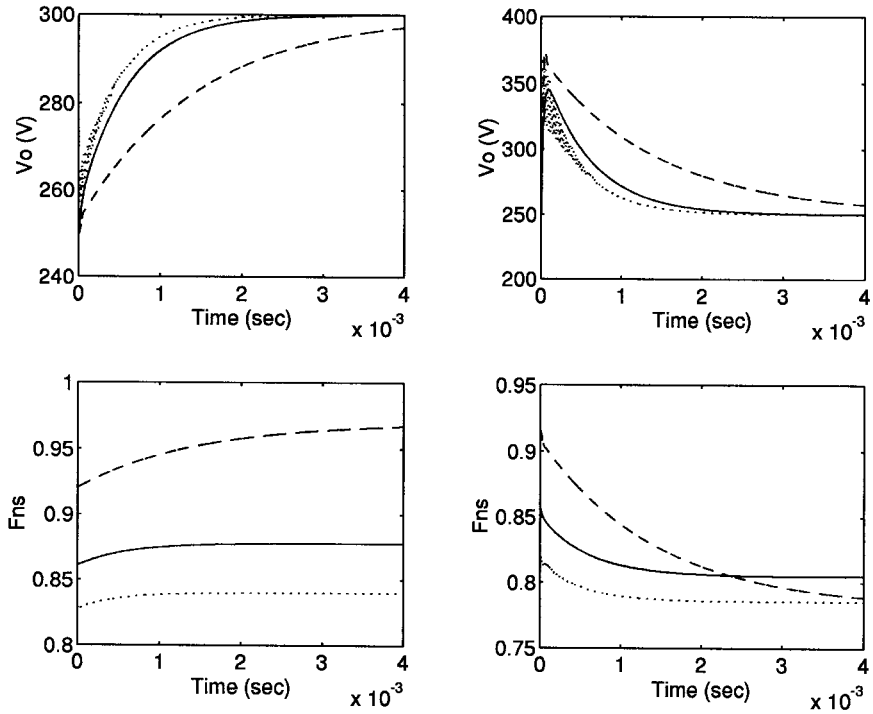

Fig. 18. Linear simulation results with phase-lag controller at different operating points $R_o = 208$ (solid), 151 (dash) and 1200 (dot) Ω: (a) Reference input step change (20%). (b) Line voltage step change (20%).

The same simulation was performed for the closed–loop system corresponding to the phase-lag controller. The time responses to 20% step change in line voltage V_{ng} and reference input r at three different operating points: $R_o = 151,\ 208$, and 1200 Ω are shown in Fig. 18. They are similar to the responses with the μ controller except that the performance is far worse for $R_o = 1200\ \Omega$. This is due to the phase-lag controller inability to provide enough attenuation to counteract the increment in the magnitude of the resonant peak of the plant at heavy loads, as shown in Fig. 15. Furthermore, as shown in Fig. 19, at $R_o = 2400\ \Omega$ the phase-lag controller fails to stabilize the system, while the μ controller can still produce acceptable performance.

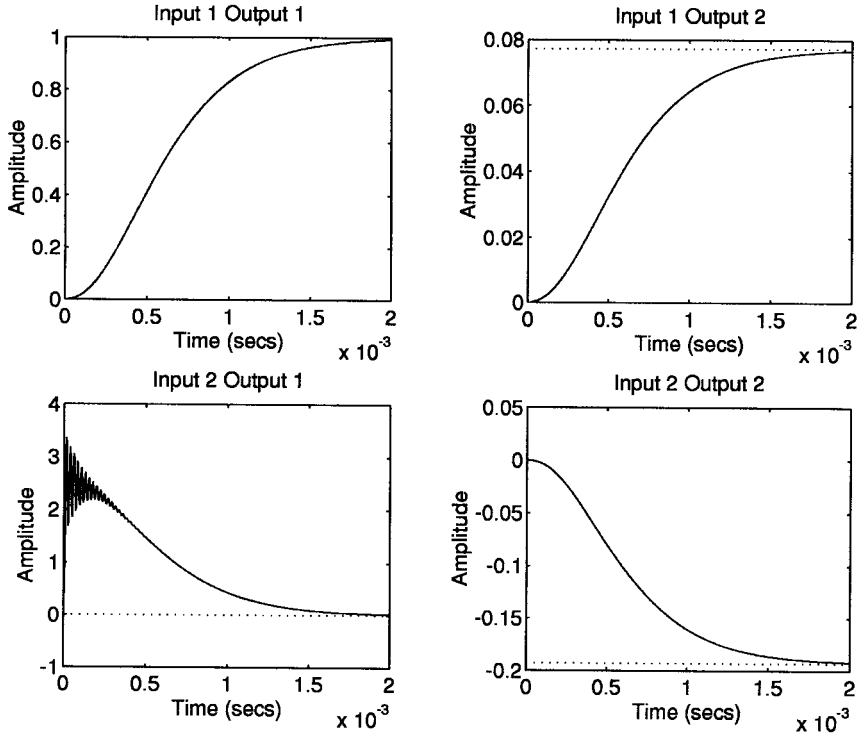

(a)

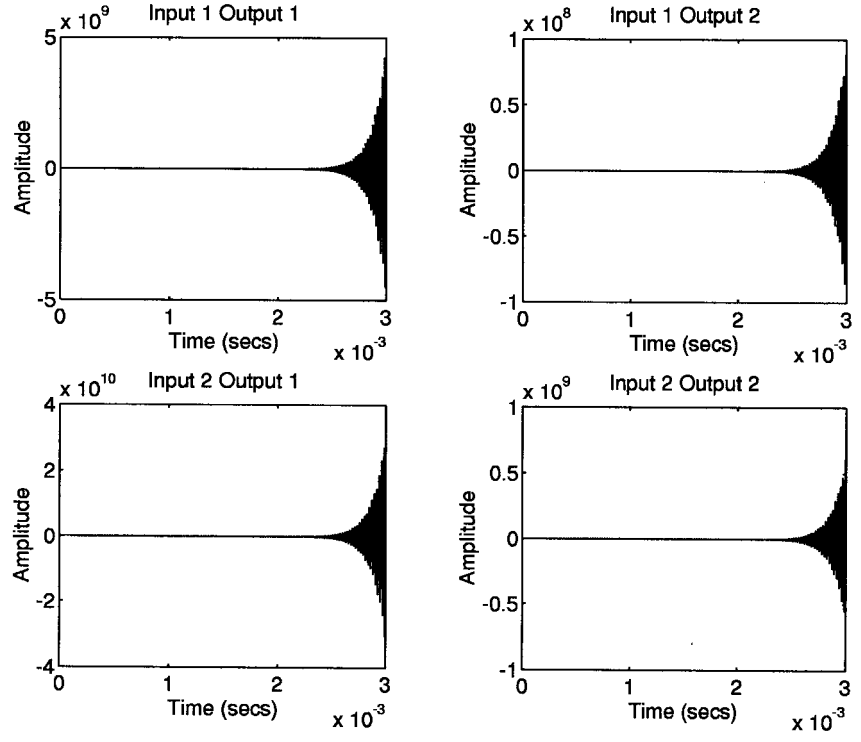

(b)

Fig. 19. Step responses of the closed-loop system at $R_o = 2400\ \Omega$: (a) μ controller (stable). (b) Phase-lag controller (unstable).

B. Nonlinear Simulations and Validation

It should be noted that the linear simulations performed in Section V-A were done using the linearized model of the converter. While linear simulations at different load conditions can usually provide an approximate evaluation of load regulation performance, this is usually insufficient to assess the performance of a highly nonlinear system such as the converter. Thus, to further validate our results, a nonlinear simulation of the PRC circuit was performed using P-Spice. The closed-loop system was obtained by first realizing the transfer function (19) using operational amplifiers and then connecting this controller to the converter.

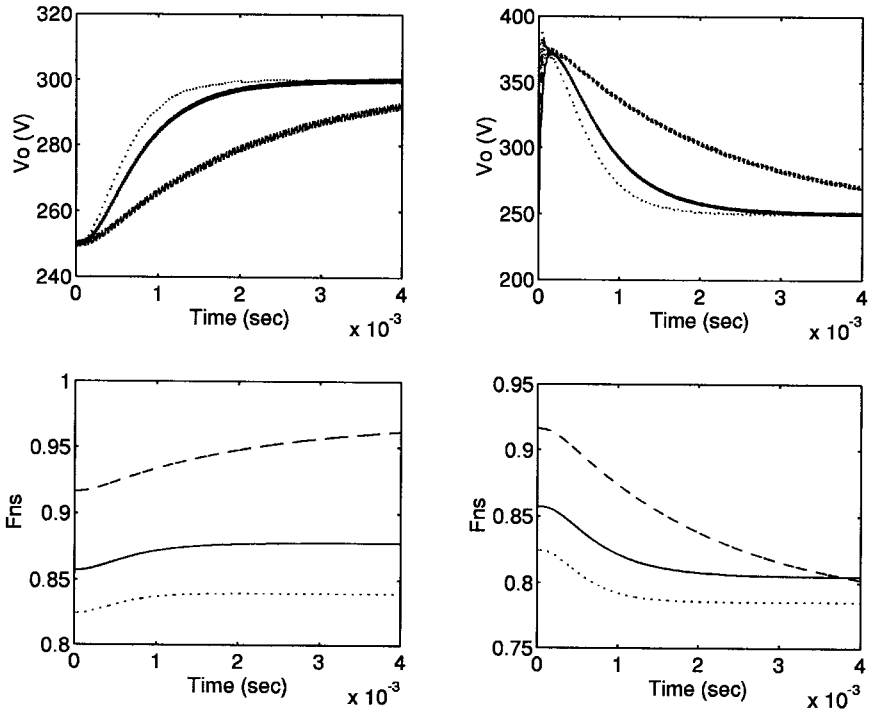

Fig. 20. Nonlinear simulation results with μ controller at different operating points $R_o = 208$ (solid), 151 (dash) and 1200 (dot) Ω: (a) Reference input step change (20%). (b) Line voltage step change (20%).

Fig. 20 shows the responses due to reference input and line voltage step changes. Note that these results are similar to those obtained using a linear simulation as shown in Fig. 17. In the responses to line voltage step change and reference step change, settling times are slightly larger than those in the linear simulation. The chattering observed in the output voltage is substantial, due to the periodic and switching behavior of the converter (periodic charge and discharge of capacitor).

VI. Conclusions

Due to their smaller size and lighter weight, resonant dc-to-dc converters have been the object of much attention lately. These converters have the potential to provide high-performance conversion, without some of the problems associated with classical PWM-based converters. However, realizing this potential requires a suitable control circuit, guaranteeing performance in the presence of line-input disturbances, load changes and component variations.

In this paper we address the problem of synthesizing these controllers within the framework of μ-synthesis. In order to cast our problem into this framework, uncertainties in the load and components are modeled as a single, norm-bounded, complex perturbation covering all possible plants. The design example of Section V demonstrates that different performance requirements can be easily incorporated by using suitable weights on the corresponding input and output signals and that conflicting performance specifications can be traded off by adjusting these weights. Detailed nonlinear circuit simulations show that the resulting controller fully satisfies the design objectives, meeting the performance specifications for a wide range of loads. Thus, the μ-synthesis robust control framework provides a systematic way for synthesizing controllers for resonant converters, avoiding the need for lengthy trial and error type iterations, without guarantee of success.

Acknowledgment

The authors are grateful to the reviewers for suggesting several improvements to the original manuscript.

References

[1] R. D. Middlebrook and S. Cuk, "Advances in switched-mode power conversion," in *TESLACO*, vols. 1–3, Pasadena, CA, 1981.
[2] I. Batarseh and C. Q. Lee, "Steady–state analysis of the parallel resonant converter with LLCC-type commutation network," *IEEE Trans. Power Electron.*, vol. 6, pp. 525–538, July 1991.
[3] S. Freeland, "An introduction to the principle and features of resonant power conversion," *Rockwell Int. Corp.–Autonetics ICBM Syst. Division*, Anaheim, CA, 1988.
[4] J. Kassakian and M. Schlecht, "High-frequency high-density converters for distributed power supply systems," *Proc. IEEE*, vol. 76, no. 4, Apr. 1988.
[5] I. Batarseh and R. Severns, "Resonant converter topologies with three and four energy storage elements," to appear in *IEEE Trans. Power Electron.*
[6] R. King and T. Stuart, "Inherited overload protection for the series resonant converter," *IEEE Trans. Aerospace Electron. Syst.*, pp. 820–830, Nov. 1983.
[7] R. Oruganti, "State-plane analysis of resonant converters," Ph.D. dissertation, Virginia Polytechnic Inst. State Univ., Blacksburg, Aug. 1987.
[8] R. Oruganti and F. C. Lee, "Resonant power processing: Part I—State-plane analysis," *IEEE Trans. Ind. Applicat.*, pp. 1453–1460, Nov./Dec. 1985.
[9] K. Siri and C. Q. Lee, "Design of series resonant converter with normalized state-plane diagram," *IEEE Trans. Aerospace Electron. Syst.*, vol. 22, pp. 757–763, 1986.
[10] R. L. Steigerwald, "A comparison of half-bridge resonant converter topologies," *IEEE Trans. Power Electron.*, vol. 3, pp. 174–182, 1988.
[11] V. Vorperian, "Analysis of resonant converters," Ph.D. dissertation, California Inst. Technol., Pasadena, May 1984.

[12] K. Liu, R. Oruganti, and F. C. Lee, "Quasi-resonant converters: Topologies and characteristics," *IEEE Trans. Power Electron.*, vol. 2, pp. 62–71, 1987.
[13] I. Batarseh, "Steady-state analysis and design of high-order resonant converters," Ph.D. dissertation, Univ. Illinois-Chicago, June 1990.
[14] S. Johnson and Erickson, "Steady-state analysis and design of the parallel resonant converters," in *Proc. IEEE PESC'86*, 1986, pp. 154–165.
[15] C. Q. Lee and I. Batarseh, "Performance characteristics of parallel resonant converter," *Electron. Lett.*, vol. 23, pp. 1273–1274, Nov. 1987.
[16] R. Oruganti and F. C. Lee, "State-plane analysis of parallel resonant converter," in *Proc. IEEE PESC'85*, 1985, pp. 56–73.
[17] P. Todd and R. Lutz, "A practical parallel loaded resonant power supply," in *Proc. IEEE APEC'86*, Apr. 1986, pp. 90–97.
[18] A. S. Bhat and S. B. Dewan, "A generalized approach for the steady-state analysis of resonant converters," in *Proc. IEEE-APEC'86*, 1986, pp. 664–671.
[19] N. Femia, G. Spagnuolo, and V. Tucci, "State-space models and order reduction for dc–dc switching converters in discontinuous modes," *IEEE Trans. Power Electron.*, vol. 10, Nov. 1995.
[20] D. Maksimovic and S. Cuk, "A unified analysis of PWM converters in discontinuous modes," *IEEE Trans. Power Electron.*, vol. 6, pp. 476–490, July 1991.
[21] G. B. Joung and G. H. Cho, "Modeling of quantum parallel resonant converters—A new parallel resonant converters controlled by integral cycle mode," in *Proc. IEEE PESC'89*, 1989, pp. 744–751.
[22] R. Oruganti and F. C. Lee, "Resonant power processing: Part II–Methods of control," *IEEE Trans. Ind. Applicat.*, pp. 1461–1471, Nov./Dec. 1985.
[23] K. Siri and C. Q. Lee, "State-plane approach to frequency response of resonant converters," in *Proc. Inst. Elect. Eng. Electron. Circuits Syst.*, vol. 138, pt. G, no. 3, pp. 557–563, Oct. 1991.
[24] A. Packard and J. C. Doyle, "The complex structured uncertainties," *Automat.*, vol. 29, no. 1, pp. 71–109, 1993.
[25] A. Packard, J. C. Doyle, and G. Balas, "Linear multivariable robust control with a μ perspective," *Trans. ASME*, vol. 115, pp. 426–437, June 1993.
[26] G. Franklin, D. Powell, and M. Workman, *Digital Control of Dynamic Systems*. Reading, MA: Addison-Wesley, 1990.
[27] G. J. Balas *et al.*, "μ-analysis and synthesis toolbox," Version 2.0, MUSYN Inc. and The MathWorks, Inc., June 1993.
[28] P. Lundstrom, S. Skogestad, and Z.-Q. Wang, "Uncertainty weight selection for H-∞ and μ-control methods," in *Proc. IEEE Conf. Decision Contr.*, Brighton, U.K., Dec. 1991.
[29] J. C. Doyle, "Analysis of feedback systems with structured uncertainties," *Proc. Inst. Elect. Eng.*, vol. 129, pt. D, no. 6, 1982, pp. 242–250.
[30] M. G. Safonov, "Stability margins of diagonally perturbed multivariable feedback systems," in *Proc. Inst. Elect. Eng.*, vol. 129, pt. D, no. 6, 1982, pp. 251–255.
[31] M. G. Safonov and M. Athans, "A multiloop generalization of the circle criterion for stability margin analysis," *IEEE Trans. Automat. Contr.*, vol. AC-26, pp. 415–422, 1981.
[32] R. Y. Chiang and M. G. Safonov, "Robust control toolbox," Version 2.0, The MathWorks, Inc., Aug. 1992.
[33] S. Skogestad, M. Morari, and J. C. Doyle, "Robust control of ill-conditioned plants: High-purity distillation," *IEEE Trans. Automat. Contr.*, vol. AC-33, pp. 1092–1105, 1988.
[34] P. Lundstrom, S. Skogestad, and Z.-Q. Wang, "Performance weight selection for H-∞ and μ-control method," *Trans. Inst. Meas. Contr.*, vol. 13, no. 5, pp. 241–252, 1991.
[35] M. Sznaier and P. Dorato, "Multiobjective robust control," Session FA–2, in *Proc. 33rd IEEE Conf. Decision Contr.*, Lake Buena Vista, FL, Dec. 14–16, 1994, pp. 2672–2707.

Juanyu Bu (S'96) was born in China on July 4, 1974. He received the B.S. degree in automatic control from the University of Science and Technology of China in 1992, and the M.S. degree in electrical engineering in 1994 from the Pennsylvania State University, University Park, where he is currently working toward the Ph.D. degree.

He also serves as a Research Assistant to Dr. M. Sznaier in Control and System Lab at Pennsylvania State University. His research interests include robust and optimal control design, and control applications on power electronics, performance analysis, and simulations.

Mr. Bu is Member of Phi Kappa Phi.

Mario Sznaier (S'89–M'89) received the Ingeniero Electronico and Ingeniero en Sistemas de Computacion degrees from the Universidad de la Republica, Uruguay, in 1983 and 1984 respectively, and the M.S.E.E. and Ph.D. degrees from the University of Washington, Seattle, in 1986 and 1989, respectively.

He spent the year 1990 as a Research Fellow in Electrical Engineering at the California Institute of Technology, Pasadena. From 1991 to 1993, he was an Assistant Professor of Electrical Engineering at the University of Central Florida (UCF), Orlando. In 1993, he joined the Department of Electrical Engineering at the Pennsylvania State University, University Park, where he is currently an Associate Professor. His research interests include multiobjective robust control, l^1 and $\mathcal{H}_\infty$ control theory, and applications of robust control to power electronics.

Dr. Sznaier is a Member of SIAM, Tau Beta Pi, and Eta Kappa Nu. From 1992 to 1993, he served as the Faculty Advisor to the IEEE Student Branch at UCF, and since 1993 has been a Coadvisor to Penn State's IEEE Student Branch. He is also serving as the current Chair of the Central Pennsylvania IEEE Chapter. He was a Member of the program and organizing committees for the 1994 IEEE Conference on Decision and Control and is a Member of the Control Systems Society Conference Editorial Board. In 1992, he was awarded a National Science Foundation Research Initiation Award for his research on robust control of systems under mixed time/frequency domain performance specifications.

Zi-Qin Wang was born in China on January 13, 1963. He received the B.S. degree in power engineering from the Wuhan Institute of Hydraulic and Electric Engineering in 1983, and the M.S. and Ph.D. degrees in control engineering from the Southeast University (formerly Nanjing Institute of Technology) in 1986 and 1990, respectively.

He was with the faculty at the Southeast University and a Norwegian Research Fellow at the Norwegian Institute of Technology, Trondheim. He is presently a Post-Doctoral Researcher at Pennsylvania State University, University Park. His research interests include robust and nonlinear control design, neural network for control, discrete-event dynamic systems, and industrial applications.

Issa Batarseh (S'83–M'91–SM'92) received the B.S., M.S., and Ph.D. degrees from the University of Illinois at Chicago in 1982, 1985, and 1990, respectively, all in electrical engineering.

He was a visiting Assistant Professor in the Electrical Engineering Department at Purdue University, West Lafayette, IN, from 1989 to 1990. In August 1991, he joined the Department of Electrical and Computer Engineering at the University of Central Florida, Orlando, where he is now an Associate Professor. His research interests include power electronics, PWM and high-frequency resonant converters, power factor correction circuits, and small signal modeling of dc-to-dc resonant converters.

Dr. Batarseh is a Coadvisor for the IEEE Student Chapter and he is a Member of Tau Beta Pi and Eta Kappa Nu. From 1991 to 1993, he served as Advisor to Eta Kappa Nu at the University of Central Florida. He is a registered Professional Engineer in Florida. He has served on the program committees of IEEE APEC, PESC, IECON, and IAS.